Sn-Induced Phase Stabilization and Enhanced Thermal Stability of κ-Ga$_2$O$_3$ Grown by Mist Chemical Vapor Deposition

Ha Young Kang,[†] Habin Kang,[†] Eunhye Lee,[†] Gyeong Ryul Lee, and Roy Byung Kyu Chung*

ACCESS | 📊 Metrics & More | 📰 Article Recommendations | 🆂ℹ Supporting Information

ABSTRACT: Tin (Sn)-doped orthorhombic gallium oxide (κ-Ga$_2$O$_3$) films were grown on (0001) sapphire by mist chemical vapor deposition. It is known that κ-Ga$_2$O$_3$ is more stable than α-Ga$_2$O$_3$ (corundum) but less stable than β-Ga$_2$O$_3$ (monoclinic). This thermodynamic stability means an optimal growth temperature (T_g) of the κ-phase (600−650 °C) is also in between the two. At first, it was observed that Sn doping induced the κ-phase during the growth of the β-phase (T_g = 700 °C). Interestingly, Sn could also promote the κ-phase even under the growth condition that strongly favors the α-phase (T_g = 450 °C). The postgrowth annealing tests at 800−1000 °C showed that the thermal stability of the κ-phase depends on the Sn concentration. The higher the Sn concentration, the more stable the phase. The one with the highest Sn content showed no phase transition from κ to β after annealing at 800, 900, and 1000 °C for 30 min each. This enhancement of thermal stability promises more reliable high-power and high-frequency devices for which κ-Ga$_2$O$_3$ is suitable. Although there was no correlation between Sn-induced phase stabilization and the crystal quality, cathodoluminescence revealed that increasing Sn concentration led to the strong suppression of the radiative recombination at 340 nm from the vacancy-related donor−acceptor pairs. This observation suggests that the phase stabilization by Sn could be related to a specific Ga site Sn replaces in the orthorhombic structure.
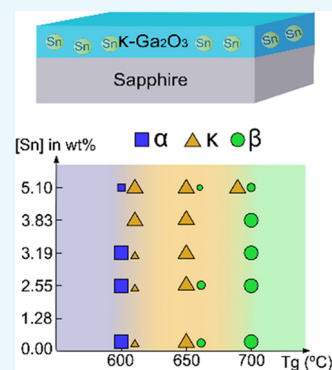
1. INTRODUCTION

Owing to the promising material properties for high-power and high-speed electronics, wide bandgap (WBG) materials such as silicon carbide (SiC) and gallium nitride (GaN) have been extensively studied over the past two decades.[1−3] Gallium oxide (Ga$_2$O$_3$) is considered a next-generation WBG material for various applications, where GaN and SiC are not suitable due to their intrinsic limitations. Ga$_2$O$_3$ is attractive as a high-power device because it has an even larger bandgap (>4.5 eV) and high breakdown field (∼8 MV/cm) compared to GaN and SiC.[4−6] There have been some interesting studies using nanoscale Ga$_2$O$_3$ as well.[7−10] However, more importantly, thermodynamically stable β-Ga$_2$O$_3$ (monoclinic) can be grown as a single crystal substrate for homoepitaxial devices with a very low dislocation density (<10^4 cm^{-2}).[11,12] This promises a commercially viable high-performance power device. Simultaneously, metastable phases such as α (corundum) and κ (orthorhombic) phases have drawn a lot of interest lately because of their unique properties.[13−15] The orthorhombic κ-phase is especially attractive as it is known to be ferroelectric and has a large spontaneous polarization (∼0.23 C/m^2), possibly an order of magnitude larger than that of III−V semiconductors such as GaN (0.029 C/m^2) and AlN (0.081 C/m^2).[14−16] Therefore, κ-Ga$_2$O$_3$ has the potential for a high-frequency and high-power device beyond GaN-based high electron mobility transistors.[17]

Compared to the progress that has been made on α- and β-phases, however, research on the κ-phase is still in its infancy.

Some of the early growth studies had reported the κ-phase (space group: P$_{na}$2$_1$) as the hexagonal ε-phase (space group: P6$_3$mc). Recently, it was found that the ε-phase actually consists of 120°-rotated nanoscale κ-phase domains.[18,19] In an effort to improve the structural quality, the impacts of different substrates (sapphire, GaN, AlN, SrTiO$_3$, yttria-stabilized ZrO$_2$, and MgO) on the epitaxial growth have been investigated.[19−23] In addition to the crystal quality, the thermal stability of this metastable phase needs to be enhanced for the long-term reliability of a device operating under an extreme environment (i.e., high temperature and high pressure). Recently, several research groups reported that the introduction of elemental Sn during a Ga$_2$O$_3$ growth could facilitate the preferential growth of the κ-phase.[24,25] So far, this phenomenon has been observed with physical vapor techniques such as pulsed laser deposition (PLD) and molecular beam epitaxy (MBE) but not with chemical vapor techniques to the best of our knowledge. At least with the physical vapor methods, earlier studies correlated this phenomenon with the surfactant effect or metal-exchange
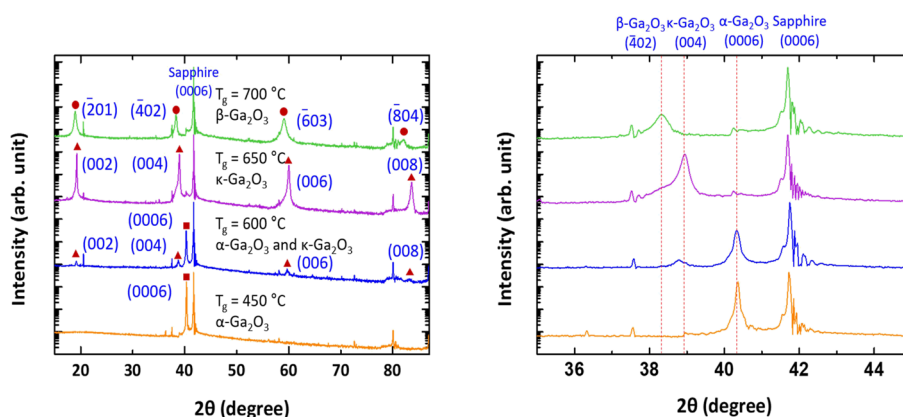
Figure 1. XRD 2θ-ω scans of Ga_2O_3 samples grown at various T_g values (red solid circle: β-Ga_2O_3, red solid triangle: κ-Ga_2O_3, and red solid square: α-Ga_2O_3)
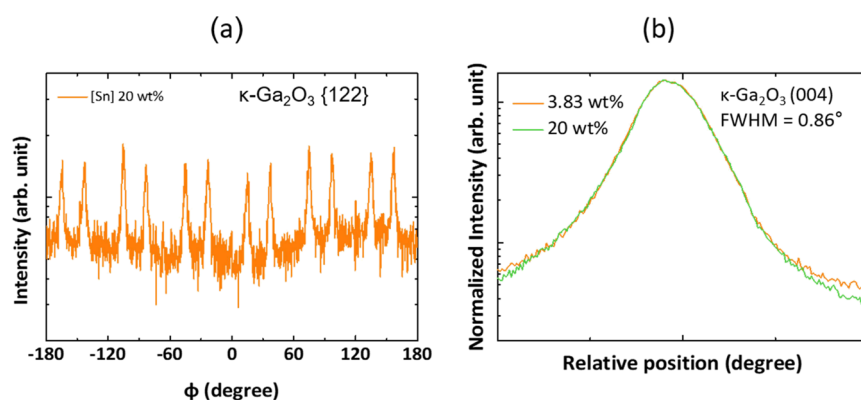

Figure 2. (a) φ-scan of $\{122\}$ κ-Ga_2O_3 and (b) rocking curve of (004) κ-Ga_2O_3 with two different Sn contents (3.83 and 20 wt %).

catalysis by Sn. The exact mechanism on the Sn-induced phase stabilization of κ-Ga_2O_3 remains elusive.

In this work, we investigated the Sn-induced phase stabilization of κ-Ga_2O_3 and the thermal stability of the films grown by mist chemical vapor deposition (CVD). Various growth experiments and analyses were carried out to gain more insights into the role of Sn in phase stabilization.

2. RESULTS AND DISCUSSION

2.1. Growth Characterizations of Ga_2O_3 Grown by Mist CVD. Figure 2 shows the T_g-dependent phase change in lightly Sn-doped Ga_2O_3 films. At T_g lower than 600 °C, the α-phase is dominant (Figure 1). A typical T_g for a pure α-phase is 450 °C with our mist CVD. Around 600 to 650 °C, the κ-phase becomes the dominant phase, but the α- and β-phases could also be observed in some cases as illustrated in Figure 2(b). A further increase of T_g above 700 °C results in single-phase β-Ga_2O_3. This temperature dependence is consistent with the enthalpy of formation (ΔH_f), which predicts α (ΔH_f = −9.8 eV per formula unit) < κ < β (ΔH_f = −10.1 to −9.9 eV per formula unit) in the increasing order of thermodynamic stability.[26] Despite the differences in the crystal structure, Ga_2O_3 can be grown on sapphire (α-Al_2O_3) with a different crystal structure as Figure 2 indicates.[16,21] Because of the identical crystal structure, the on-axis (0006) reflection of α-Ga_2O_3 typically shows a narrow rocking curve (see Figure S1). Other phases, on the other hand, display a relatively broad rocking curve. In the case of the κ-phase, a buffer layer forms on the surface because of the dissimilarity.[19,27] Figure 3(a)
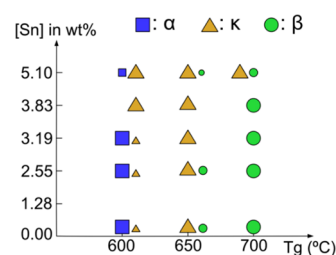

Figure 3. Mapping the phase of Ga_2O_3 as a function of $[Sn]$ (in wt %) and T_g. A size difference of each shape indicates the relative dominance of a certain phase when two phases coexist.

shows a φ-scan of (122) κ-Ga_2O_3. These 12 peaks are the key feature related to three 120°-rotated orthorhombic domains, confirming the growth of single-phase κ-Ga_2O_3. Rocking curves of the (004) reflection of κ-Ga_2O_3 with different Sn concentrations are shown in Figure 3(b). A typical full width at half maximum (FWHM) value of the κ-phase samples is ~0.86°, higher than that of the PLD, metal organic chemical vapor deposition (MOCVD), or MBE samples (0.3−0.6°).[24,25,28] For a heteroepitaxial growth, it is not unusual that a thicker film contains fewer dislocations than a thinner film through the dislocation annihilation process.[29,30] Higher FWHM values observed from our samples (~250 nm) indicate a higher density of defects than the PLD-, MOCVD-, or MBE-grown ones (500−1000 nm) reported by others, but the difference is partly caused by the thickness-related defect reduction. Overall, the growth behavior of the κ-phase on

sapphire does not seem to be heavily dependent on a growth method within the growth results reported so far. This means that the effect of Sn doping on the structural property could also be agnostic to a growth method. In ref 14, the FWHM value of (002) reflection for a mist-CVD-grown κ-phase film with a similar thickness was ~0.72 arcsec. As noted earlier, it has been demonstrated that α-Ga$_2$O$_3$ grown on sapphire exhibits a higher crystalline quality than the other phases due to the same crystal structure. The (006) reflection of α-Ga$_2$O$_3$ was also measured (Figure S1) for a sanity check of our mist CVD system. The FWHM of the α-phase was ~0.029°, comparable to the values reported by others.[31−33] Transmittance and Tauc plots in Figure S2 demonstrate high crystalline-quality materials with the optical bandgap values consistent with the reported values for all three phases grown with our mist CVD.[14] Therefore, the material quality of our mist-CVD-grown samples is comparable to that of κ-Ga$_2$O$_3$ reported by others. Figure 3(b) also indicates that FWHM does not vary much with the amounts of Sn, suggesting that the phase stabilization does not affect the crystal quality. It is also worthwhile to mention that the κ-phase did not show any secondary phase or alloying effect even with [Sn] = 20 wt %, which may be an indication of limited incorporation of Sn during the growth. Details of the phase stabilization are discussed in the following sections. Under the optimal T_g (650 °C) for the κ-phase, the Sn concentration ([Sn]/[Ga] in %wt) in the solution was varied as summarized in Table 1. The

Table 1. Summary of Growth Conditions

film thickness	~250 nm
substrate	c-plane sapphire
growth temperature (T_g)	450−700 °C
growth pressure (Torr)	765
carrier gas	N$_2$
solution	Ga(acac)$_3$, SnCl$_2$·2H$_2$O, deionized water, HCl, and H$_2$O$_2$
Sn concentration ([Sn], wt %)	0,1.28, 2.55, 3.19, 3.83, 5.10, 6.38, and 20

substitutional Sn (Sn$_{Ga}$) is known to be a donor in α- and β-phases.[34−36] However, none of the κ-phase samples doped with Sn in this study exhibited conductivity. Further study is necessary to understand the doping efficiency of Sn in κ-Ga$_2$O$_3$.

2.2. Phase Stabilization via Sn Doping. While Sn was ineffective as a donor, it seemed responsible for the stabilization of metastable κ-Ga$_2$O$_3$ over α- and β-phases. Figure 4 summarizes the results where the square, triangle, and circle indicate α-, κ-, and β-phases, respectively. Although there
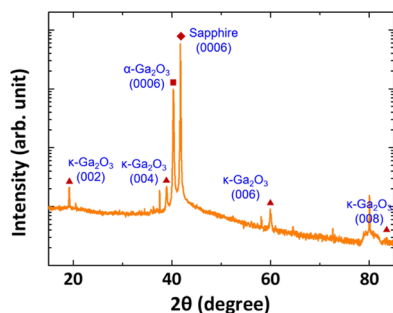

Figure 4. 2θ-ω scans of Ga$_2$O$_3$ (T_g = 450 °C) with [Sn] = 3.83 wt %.

were some samples exhibiting inconsistency, the overall trend was that increasing [Sn]/[Ga] resulted in more κ-phase-dominant films for 600 °C $\leq T_g \leq$ 700 °C. Surprisingly, Sn doping of Ga$_2$O$_3$ grown at T_g = 450 °C could also induce the κ-phase within the α-phase as shown in Figure 5. Therefore, Sn
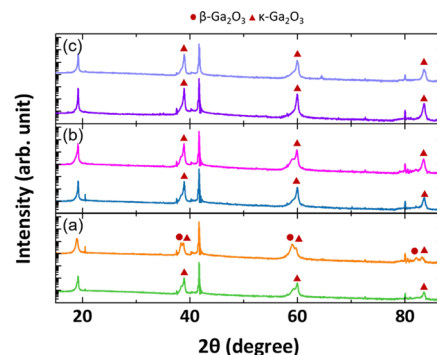

Figure 5. 2θ-ω scans of κ-Ga$_2$O$_3$ with (a) [Sn] = 0, (b) [Sn] = 3.83, and (c) [Sn] = 20 wt % after the last annealing step at 1000 °C.

makes the κ-phase more thermally stable under a high-temperature environment (that favors the β-phase); it also lowers the kinetic energy barrier required to form the κ-phase under a low-temperature environment (that favors the α-phase). It is important to note that the Sn-doped α-phase was conductive (Hall concentration−5 × 10^{18} cm^{-3} and Hall mobility ~1.99 cm^2/Vs) with [Sn] = 2.55 wt %, but it became insulating at a higher Sn concentration as the κ-phase emerges. This could also be an indication that the dominant oxidation state of Sn may be Sn^{2+}, which could act as a compensator in the κ-phase. Exploring possible configurations of Sn in the κ-phase may shed some light on how this metastable phase becomes stabilized over α- and β-phases even under the growth conditions that normally favor these phases.

The thermal stability of Sn-doped κ-Ga$_2$O$_3$ was further assessed with the postgrowth annealing tests at 800−1000 °C. Each sample was annealed at 800 °C for 30 min, 900 °C for 30 min, and 1000 °C for 30 min. Between each annealing process, the phase change was monitored by X-ray diffraction (XRD). Figure 6 shows the XRD profiles of as-is and after 1000 °C annealing. Figure 6(a) shows the undoped κ-Ga$_2$O$_3$ grown at
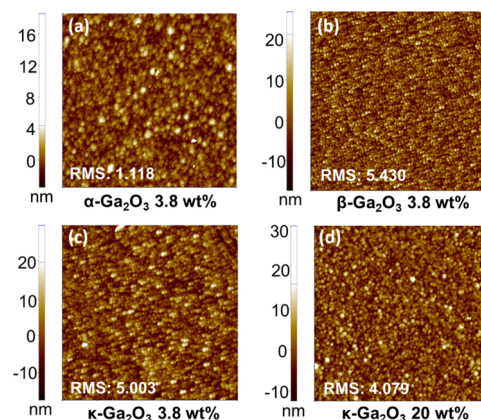

Figure 6. 5 × 5 μm^2 AFM images of (a) α-Ga$_2$O$_3$ (mixed with the κ-phase) with [Sn] = 3.83 wt %, (b) β-Ga$_2$O$_3$ with [Sn] = 3.83 wt %, (c) κ-Ga$_2$O$_3$ with [Sn] = 3.83 wt %, and (d) κ-Ga$_2$O$_3$ with [Sn] = 20 wt %.

650 °C. The XRD 2θ-ω scan indicates that this particular sample contains both β- and κ-phases. Since the $(\bar{2}01)$ peak of the β-phase and the (004) peak of the κ-phase are very close to each other, higher-order peaks are also monitored. After annealing at 1000 °C for 30 min, the $(\bar{8}04)$ and (008) peaks are clearly observed with the relative intensity of the β-phase quickly rising. As [Sn] increased to 3.19 wt %, the film started showing a sign of β-phase suppression. At [Sn] = 20 wt %, the XRD profile barely changed after annealing at 1000 °C. Improving the thermal stability of the κ-phase via Sn doping could open up new opportunities for high-power and high-frequency electronics operating in an extreme environment (operation temperature up to 1000 °C or beyond).[3]

2.3. Role of Sn in κ-Ga$_2$O$_3$. As mentioned earlier, several groups have reported on the Sn-assisted κ-Ga$_2$O$_3$ growth via MBE and PLD. In the case of PLD, the surfactant-mediated epitaxy was attributed to the improved crystalline quality of the κ-phase.[24] It was also suggested that the preferential growth of the κ-phase over the β-phase was correlated with the surfactant effect induced by Sn. A surfactant-mediated growth generally accompanies surface smoothening along with a surfactant-rich layer at/near the surface but not in the bulk region.[37,38] Atomic force microscopy (AFM) images in Figure 7(a−c) show that
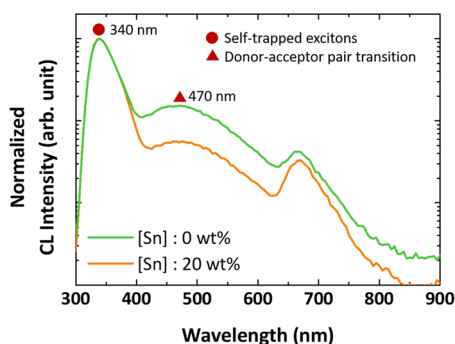

Figure 7. CL spectra of (a) undoped κ-Ga$_2$O$_3$ (green) and (b) κ-Ga$_2$O$_3$ with [Sn] = 20 wt % (orange).

the root-mean-square roughness of the κ-phase (5.003 nm) is lower than that of the β-phase (5.430 nm) but higher than that of the α-phase (1.118 nm). The morphology of the κ-phase indicates larger domains on average compared to that of the β-phase. Since all three films contain Sn, it is more likely that the differences in roughness come from an epitaxial relation to the underlying sapphire substrate. Figure 7(d) illustrates that

higher [Sn] creates a smoother surface, suggesting that Sn does act as a surfactant like In.[38] However, it is not clear whether or not the surface effect is the reason for the phase stabilization, which is concentration dependent according to Figure 5. Secondary ion mass spectrometry (SIMS) profiles in Figure S3(a−c) suggest the presence of Sn in the bulk region. Higher Sn concentration near the surface in the SIMS profile is likely an artifact due to the surface contamination as all four samples in Figure S3 exhibit a similar feature. The X-ray photoemission spectroscopy (XPS) spectrum of the surface showed no Sn-related signal. In Figure S3, it is also noticeable that the amount of Sn varies accordingly with the concentration of Sn up to [Sn] = 20 wt % in the mist solution, suggesting that the phase stabilization mechanism is not directly related to the surfactant effect. Even with [Sn] = 20 wt %, the actual Sn concentration in κ-Ga$_2$O$_3$ is likely 10^{19}–10^{20} cm^{-3} given that the α-phase with [Sn] = 2.55 wt % has a carrier concentration of 5×10^{18} cm^{-3}. The similar SIMS result from the α-phase with [Sn] = 2.55 wt % in Figure S3(d) also indicates that there is no drastic difference in the incorporation efficiency of Sn between the two phases. Therefore, it is unlikely that there is an alloying effect with [Sn] = 20 wt %. There was no structural indication of alloying either. Others have suggested that the metal-exchange catalytic effect between Ga and Sn (or In) could widen the growth window for a metastable κ-phase during MBE growth.[25,39] It was argued that the catalytic elements like Sn and In with higher oxidation efficiency give up the oxygen atoms to Ga$_2$O at the growth surface to form Ga$_2$O$_3$ (i.e., Ga$_2$O + 2SnO$_2$ → Ga$_2$O$_3$ + 2SnO), where Ga replacing Sn or In is thermodynamically favorable. Kracht et al. also speculated that Sn on the octahedral Ga site could structurally promote the growth of κ-Ga$_2$O$_3$.[25]

Interestingly, the emission characteristics changed with increasing [Sn] according to the cathodoluminescence (CL) analysis in Figure 8. The CL spectrum of undoped κ-Ga$_2$O$_3$ is almost identical to that of α- and β-Ga$_2$O$_3$ (see Figure S4). The only difference is the emission energy because of the difference in the bandgap between the two phases. Therefore, it is likely that the origin of each emission peak from the κ-phase is identical to that from the β-phase.[40,41] The main ultraviolet emission at about 340 nm has been attributed to the recombination between the electrons and self-trapped holes or the recombination of self-trapped excitons. The emission at 470 nm comes from the donor−acceptor pairs (DAPs) in which the anion and cation vacancies are responsible for the electrons and holes, respectively. The red emission at 680 nm is likely a second-order peak of the emission at 340 nm. For
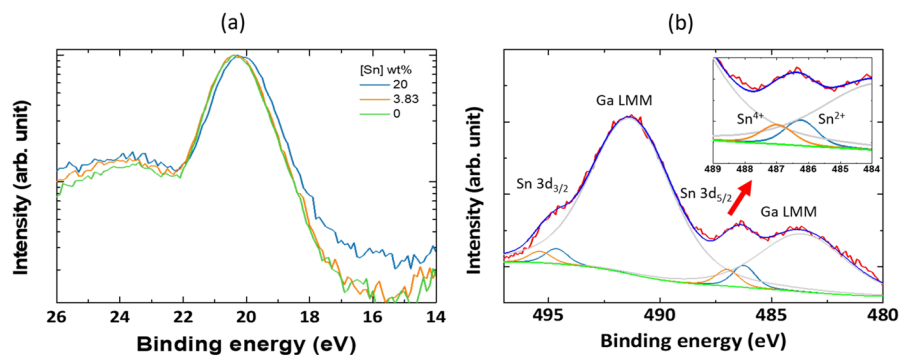

Figure 8. XPS spectra of (a) Ga 3d$_{3/2}$ from κ-Ga$_2$O$_3$ with [Sn] = 0, 3.83, and 20 wt % and (b) Sn 3d$_{3/2}$ and 3d$_{5/2}$ from κ-Ga$_2$O$_3$ with [Sn] = 20 wt %.

comparison, the CL spectra of undoped and Sn-doped ($[Sn]$ = 20 wt %) samples are normalized to the 340 nm peak. The normalized spectra clearly show the suppression of blue emission in the Sn-doped sample. Sn interfering with the DAP transitions could indicate substitutional Sn (Sn_{Ga}) on the Ga site.[39,42] This speculation was further supported by the XPS analysis of Ga 3d and Sn 3d peaks in Figure 9. With increasing
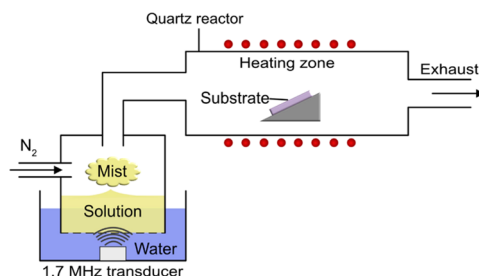

Figure 9. Schematic drawing of the mist CVD system.

$[Sn]$, a shoulder peak on the lower binding energy side becomes more obvious in Figure 9(a), suggesting that Ga is being substituted by another element. In the case of the β-phase, Sn is expected to replace Ga on an octahedral site and donates an electron.[42] Whether or not Sn replaces an octahedral site in κ-Ga$_2$O$_3$ requires a more theoretical investigation. As mentioned earlier, none of the κ-phase samples exhibited conductivity. One possibility is that Sn_{Ga} exists as the Sn^{2+} oxidation state as it replaces Ga. At first, an Sn-related XPS peak could not be observed near the surface even for the sample with the highest $[Sn]$, suggesting that there is no Sn accumulation at the growth front. Only after etching a portion of the film near the surface, XPS peaks of Sn could be detected. In comparison with the XPS profile of an undoped sample shown in Figure S5, the one in Figure 9(b) exhibits one distinctive peak around 486 eV and a shoulder peak around 492 eV. Although the peaks are strongly overlapped, the XPS signal at a binding energy of 486 eV could be fitted with two peaks with the binding energies at ~486.2 and 487 eV, which can be associated with Sn^{2+} and Sn^{4+}, respectively, in an Sn−O compound.[43] Sn being in the 2+ charge state is compatible with the metal-exchange scenario, which predicts the formation of SnO after the growth. How Sn_{Ga} and its oxidation state are related to the phase stabilization as well as the metal-exchange catalysis requires further investigation. This work, however, does suggest that the phase stabilization is agnostic to a growth method. It seems more likely that a structure with a certain defect configuration may be the driving force for the preferential growth of κ-Ga$_2$O$_3$.[44]

3. CONCLUSIONS

In summary, Sn doping of metastable κ-Ga$_2$O$_3$ enhanced its thermal stability so that the growth window in terms of T_g could be widened to both lower and higher temperature ranges than its nominal T_g. Without Sn, on the other hand, the phase control was very temperature-sensitive. Sn-doped κ-Ga$_2$O$_3$ ($[Sn]$ = 20 wt %) exhibited no phase transition even after annealing for 90 min at 800, 900, and 1000 °C (30 min each), the temperature well above typical T_g (650 °C) of κ-Ga$_2$O$_3$. While AFM and SIMS analyses exhibited little evidence of a surfactant effect or metal-exchange effect by Sn during growth by mist CVD, it was observed that Sn doping suppressed the DAP-related optical transitions according to CL. XPS analysis

indicates that Sn exists as both Sn^{2+} and Sn^{4+}, but the +2 oxidation state seems to be more dominant. This assessment is consistent with the resistive films. However, the charge compensation effect cannot be ruled out given the poor material quality of heteroepitaxial κ-Ga$_2$O$_3$. Understanding the correlation between structural stability and the charge state of Sn requires a more theoretical approach. From a practical point of view, however, our study showed a possibility of thermally stable κ-Ga$_2$O$_3$ power devices operating even under a high-temperature environment.

4. EXPERIMENTAL SECTION

κ-Ga$_2$O$_3$ (thickness−250 nm) films were grown on a sapphire substrate by mist CVD. A 0.02 M solution containing gallium acetylacetonate (Ga(acac)$_3$), SnCl$_2$-2H$_2$O, HCl, H$_2$O$_2$, and deionized water was used. The solution was prepared by adding 1.098 g of Ga(acac)$_3$ and SnCl$_2$-2H$_2$O with various weights to 150 mL of deionized water with 1.5 mL of HCl and 0.75 mL of H$_2$O$_2$. The solution was then stirred with a magnetic stirrer until no solid was observed in the solution. The solution was atomized with a 1.7 MHz transducer to generate the mist. The mist was then transferred to a quartz tube reactor by N$_2$ carrier gas as schematically depicted in Figure 1. The amount of SnCl$_2$-2H$_2$O was varied in the solution to change the concentration of Sn in Ga$_2$O$_3$ films (see Table 1). A typical growth temperature (T_g) for Ga$_2$O$_3$ was between 450 and 700 °C depending on a desired Ga$_2$O$_3$ phase. The growth conditions are summarized in Table 1. After the growth, the samples were annealed at 800 °C for 30 min, 900 °C for 30 min, and 1000 °C for 30 min (total annealing time = 90 min) in the air to investigate the impacts of Sn doping on thermal stability. The degree of phase change was assessed after each annealing step. Various analytical tools, such as XRD, SIMS, AFM, CL, XPS, and Hall measurements, were used to characterize the structural, chemical, and electrical properties of samples. Our XPS uses an Al-Kα source, which is known to generate the Ga Auger peak (Ga LMM) around 400−600 eV.

■ ASSOCIATED CONTENT

ⓢ Supporting Information

The Supporting Information is available free of charge at https://pubs.acs.org/doi/10.1021/acsomega.1c05130.

> Data showing the crystalline quality of α-Ga$_2$O$_3$ grown using the in-house mist CVD system; optical properties to assess the crystalline quality of α-, κ-, and β-Ga$_2$O$_3$ samples grown using the in-house mist CVD system; SIMS from κ- and α-phase samples for the comparison of Sn concentration; CL spectra of α-, κ-, and β-Ga$_2$O$_3$ samples; XPS profile of the undoped κ-Ga$_2$O$_3$ sample (PDF)

■ AUTHOR INFORMATION

Corresponding Author

> **Roy Byung Kyu Chung** − *Electronic Materials Science and Engineering Department, Kyungpook National University, Daegu 41566, South Korea;* ⓞ orcid.org/0000-0002-1599-5034; Email: roy.b.chung@knu.ac.kr

Authors

Ha Young Kang − *Electronic Materials Science and Engineering Department, Kyungpook National University, Daegu 41566, South Korea*

Habin Kang − *Electronic Materials Science and Engineering Department, Kyungpook National University, Daegu 41566, South Korea*

Eunhye Lee − *Electronic Materials Science and Engineering Department, Kyungpook National University, Daegu 41566, South Korea*

Gyeong Ryul Lee − *Electronic Materials Science and Engineering Department, Kyungpook National University, Daegu 41566, South Korea*

Complete contact information is available at:
https://pubs.acs.org/10.1021/acsomega.1c05130

Author Contributions

[†]H.Y.K., H.K., and E.L. contributed equally to this work.

Notes

The authors declare no competing financial interest.

■ ACKNOWLEDGMENTS

■ REFERENCES

(1) He, J.; Cheng, W.; Wang, Q.; Cheng, K.; Yu, H.; Chai, Y. Recent Advances in GaN-Based Power HEMT Devices. *Adv. Electron. Mater.* **2021**, 7, No. 2001045.

(2) She, X.; Huang, A. Q.; Lucia, O.; Ozpineci, B. Review of Silicon Carbide Power Devices and Their Applications. *IEEE Trans. Ind. Electron.* **2017**, 64, 8193−8205.

(3) Tsao, J. Y.; Chowdhury, S.; Hollis, M. A.; Jena, D.; Johnson, N. M.; Jones, K. A.; Kaplar, R. J.; Rajan, S.; Van de Walle, C. G.; Bellotti, E.; Chua, C. L.; Collazo, R.; Coltrin, M. E.; Cooper, J. A.; Evans, K. R.; Graham, S.; Grotjohn, T. A.; Heller, E. R.; Higashiwaki, M.; Islam, M. S.; Juodawlkis, P. W.; Khan, M. A.; Koehler, A. D.; Leach, J. H.; Mishra, U. K.; Nemanich, R. J.; Pilawa-Podgurski, R. C. N.; Shealy, J. B.; Sitar, Z.; Tadjer, M. J.; Witulski, A. F.; Wraback, M.; Simmons, J. A. Ultrawide-Bandgap Semiconductors: Research Opportunities and Challenges. *Adv. Electron. Mater.* **2018**, 4, No. 1600501.

(4) Pearton, S. J.; Ren, F.; Tadjer, M.; Kim, J. Perspective: Ga_2O_3 for Ultra-High Power Rectifiers and MOSFETS. *J. Appl. Phys.* **2018**, 124, 220901.

(5) Mastro, M. A.; Kuramata, A.; Calkins, J.; Kim, J.; Ren, F.; Pearton, S. J. Perspective—Opportunities and Future Directions for Ga2O3. *ECS J. Solid State Sci. Technol.* **2017**, 6, P356−P359.

(6) Masataka, H.; Kohei, S.; Hisashi, M.; Yoshinao, K.; Akinori, K.; Akito, K.; Takekazu, M.; Shigenobu, Y. Recent Progress in Ga2O3 Power Devices. *Semicond. Sci. Technol.* **2016**, 31, No. 034001.

(7) Abdullah, Q. N.; Yam, F. K.; Mohmood, K. H.; Hassan, Z.; Qaeed, M. A.; Bououdina, M.; Almessiere, M. A.; Al-Otaibi, A. L.; Abdulateef, S. A. Free Growth of One-Dimensional β-Ga_2O_3 Nanostructures Including Nanowires, Nanobelts and Nanosheets Using a Thermal Evaporation Method. *Ceram. Int.* **2016**, 42, 13343−13349.

(8) Abdullah, Q. N.; Yam, F. K.; Hassan, Z.; Bououdina, M. Growth and Conversion of β-Ga_2O_3 Nanobelts into GaN Nanowires via Catalyst-Free Chemical Vapor Deposition Technique. *Superlattices Microstruct.* **2013**, 54, 215−224.

(9) Abdullah, Q. N.; Ahmed, A. R.; Ali, A. M.; Yam, F. K.; Hassan, Z.; Bououdina, M. Novel SnO_2-Coated β-Ga_2O_3 Nanostructures for Room Temperature Hydrogen Gas Sensor. *Int. J. Hydrogen Energy* **2021**, 46, 7000−7010.

(10) Kim, J.; Tadjer, M. J.; Mastro, M. A.; Kim, J. Controlling the Threshold Voltage of β-Ga_2O_3 Field-Effect Transistors: Via Remote Fluorine Plasma Treatment. *J. Mater. Chem. C* **2019**, 7, 8855−8860.

(11) Reese, S. B.; Remo, T.; Green, J.; Zakutayev, A. How Much Will Gallium Oxide Power Electronics Cost? *Joule* **2019**, 3, 903−907.

(12) Baldini, M.; Galazka, Z.; Wagner, G. Recent Progress in the Growth of β-Ga_2O_3 for Power Electronics Applications. *Mater. Sci. Semicond. Process.* **2018**, 78, 132−146.

(13) Ahmadi, E.; Oshima, Y. Materials Issues and Devices of α- and β-Ga_2O_3. *J. Appl. Phys.* **2019**, 126, 160901.

(14) Yusa, S.; Oka, D.; Fukumura, T. High-κ Dielectric ε-Ga_2O_3 Stabilized in a Transparent Heteroepitaxial Structure Grown by Mist CVD at Atmospheric Pressure. *CrystEngComm* **2020**, 22, 381−385.

(15) Mezzadri, F.; Calestani, G.; Boschi, F.; Delmonte, D.; Bosi, M.; Fornari, R. Crystal Structure and Ferroelectric Properties of ε-Ga_2O_3 Films Grown on (0001)-Sapphire. *Inorg. Chem.* **2016**, 55, 12079−12084.

(16) Bosi, M.; Mazzolini, P.; Seravalli, L.; Fornari, R. Ga_2O_3 Polymorphs: Tailoring the Epitaxial Growth Conditions. *J. Mater. Chem. C* **2020**, 8, 10975−10992.

(17) Ranga, P.; Cho, S. B.; Mishra, R.; Krishnamoorthy, S. Highly Tunable, Polarization-Engineered Two-Dimensional Electron Gas in ε-$AlGaO_3$/ε-Ga_2O_3 Heterostructures. *Appl. Phys. Express* **2020**, 13, No. 061009.

(18) Cora, I.; Mezzadri, F.; Boschi, F.; Bosi, M.; Čaplovičová, M.; Calestani, G.; Dódony, I.; Pécz, B.; Fornari, R. The Real Structure of ε-Ga_2O_3 and Its Relation to κ-Phase. *CrystEngComm* **2017**, 19, 1509−1516.

(19) Nishinaka, H.; Komai, H.; Tahara, D.; Arata, Y.; Yoshimoto, M. Microstructures and Rotational Domains in Orthorhombic ε-Ga_2O_3 Thin Films. *Jpn. J. Appl. Phys.* **2018**, 57, No. 115601.

(20) Yao, Y.; Okur, S.; Lyle, L. A. M.; Tompa, G. S.; Salagaj, T.; Sbrockey, N.; Davis, R. F.; Porter, L. M. Growth and Characterization of α-, β-, and ε-Phases of Ga_2O_3 Using MOCVD and HVPE Techniques. *Mater. Res. Lett.* **2018**, 6, 268−275.

(21) Gottschalch, V.; Merker, S.; Blaurock, S.; Kneiß, M.; Teschner, U.; Grundmann, M.; Krautscheid, H. Heteroepitaxial Growth of α-, β-, γ- and κ-Ga_2O_3 Phases by Metalorganic Vapor Phase Epitaxy. *J. Cryst. Growth* **2019**, 510, 76−84.

(22) Shimazoe, K.; Nishinaka, H.; Arata, Y.; Tahara, D.; Yoshimoto, M. Phase Control of α- and κ-Ga_2O_3 Epitaxial Growth on $LiNbO_3$ and $LiTaO_3$ Substrates Using α-Fe_2O_3 Buffer Layers. *AIP Adv.* **2020**, 10, No. 055310.

(23) Tahara, D.; Nishinaka, H.; Morimoto, S.; Yoshimoto, M. Stoichiometric Control for Heteroepitaxial Growth of Smooth ε-Ga_2O_3 Thin Films on c-Plane AlN Templates by Mist Chemical Vapor Deposition. *Jpn. J. Appl. Phys.* **2017**, 56, No. 078004.

(24) Kneiß, M.; Hassa, A.; Splith, D.; Sturm, C.; Von Wenckstern, H.; Schultz, T.; Koch, N.; Lorenz, M.; Grundmann, M. Tin-Assisted Heteroepitaxial PLD-Growth of κ-Ga_2O_3 Thin Films with High Crystalline Quality. *APL Materials* **2019**, 7, No. 022516.

(25) Kracht, M.; Karg, A.; Schörmann, J.; Weinhold, M.; Zink, D.; Michel, F.; Rohnke, M.; Schowalter, M.; Gerken, B.; Rosenauer, A.; Klar, P. J.; Janek, J.; Eickhoff, M. Tin-Assisted Synthesis of E−Ga2O3 by Molecular Beam Epitaxy. *Phys. Rev. Appl.* **2017**, 8, No. 054002.

(26) Wang, T.; Li, W.; Ni, C.; Janotti, A. Band Gap and Band Offset of Ga_2O_3 and $(Al_xGa_{1-x})_2O_3$ Alloys. *Phys. Rev. Appl.* **2018**, 10, No. 011003.

(27) Xu, Y.; Park, J.-H.; Yao, Z.; Wolverton, C.; Razeghi, M.; Wu, J.; Dravid, V. P. Strain-Induced Metastable Phase Stabilization in Ga_2O_3 Thin Films. *ACS Appl. Mater. Interfaces* **2019**, 11, 5536−5543.

(28) Sun, H.; Li, K.-H.; Castanedo, C. G. T.; Okur, S.; Tompa, G. S.; Salagaj, T.; Lopatin, S.; Genovese, A.; Li, X. HCl Flow-Induced Phase Change of α-, β-, and ε-Ga_2O_3 Films Grown by MOCVD. *Cryst. Growth Des.* **2018**, 18, 2370−2376.

(29) Oshima, Y.; Kawara, K.; Shinohe, T.; Hitora, T.; Kasu, M.; Fujita, S. Epitaxial Lateral Overgrowth of α-Ga_2O_3 by Halide Vapor Phase Epitaxy. *APL Mater.* **2019**, 7, No. 022503.

(30) Cha, A. N.; Bang, S.; Rho, H.; Bae, H.; Jeon, D. W.; Ju, J. W.; Hong, S. K.; Ha, J. S. Effects of Nanoepitaxial Lateral Overgrowth on Growth of α-Ga2O3 by Halide Vapor Phase Epitaxy. *Appl. Phys. Lett.* **2019**, *115*, No. 091605.

(31) Xu, Y.; Cheng, Y.; Li, Z.; Chen, D.; Xu, S.; Feng, Q.; Zhu, W.; Zhang, Y.; Zhang, J.; Zhang, C.; Hao, Y. Ultrahigh-Performance Solar-Blind Photodetectors Based on High Quality Heteroepitaxial Single Crystalline B-Ga_2O_3 Film Grown by Vacuum-Free, Low-Cost Mist Chemical Vapor Deposition. *Adv. Mater. Technol.* **2021**, *6*, No. 2001296.

(32) Dang, G. T.; Kawaharamura, T.; Furuta, M.; Allen, M. W. Mist-CVD Grown Sn-Doped α-Ga_2O_3 MESFETs. *IEEE Trans. Electron Devices* **2015**, *62*, 3640−3644.

(33) Muazzam, U. U.; Chavan, P.; Raghavan, S.; Muralidharan, R.; Nath, D. N. Optical Properties of Mist CVD Grown α-Ga_2O_3. *IEEE Photonics Technol. Lett.* **2020**, *32*, 422−425.

(34) Tadjer, M. J.; Lyons, J. L.; Nepal, N.; Freitas, J. A.; Koehler, A. D.; Foster, G. M. Editors' Choice—Review—Theory and Characterization of Doping and Defects in β-Ga2O3. *ECS J. Solid State Sci. Technol.* **2019**, *8*, Q3187−Q3194.

(35) Dong, L.; Yu, J.; Zhang, Y.; Jia, R. Elements (Si, Sn, and Mg) Doped α-Ga_2O_3: First-Principles Investigations and Predictions. *Comput. Mater. Sci.* **2019**, *156*, 273−279.

(36) Zhang, Y.; Alema, F.; Mauze, A.; Koksaldi, O. S.; Miller, R.; Osinsky, A.; Speck, J. S. MOCVD Grown Epitaxial β-Ga_2O_3 Thin Film with an Electron Mobility of 176 Cm^2/Vs at Room Temperature. *APL Mater.* **2019**, *7*, No. 022506.

(37) Widmann, F.; Daudin, B.; Feuillet, G.; Pelekanos, N.; Rouvière, J. L. Improved Quality GaN Grown by Molecular Beam Epitaxy Using In as a Surfactant. *Appl. Phys. Lett.* **1998**, *73*, 2642−2644.

(38) Chen, H.; Feenstra, R. M.; Northrup, J. E.; Zywietz, T.; Neugebauer, J.; Greve, D. W. Surface Structures and Growth Kinetics of InGaN(0001) Grown by Molecular Beam Epitaxy. *J. Vac. Sci. Technol. B* **2000**, *18*, 2284.

(39) Vogt, P.; Brandt, O.; Riechert, H.; Lähnemann, J.; Bierwagen, O. Metal-Exchange Catalysis in the Growth of Sesquioxides: Towards Heterostructures of Transparent Oxide Semiconductors. *Phys. Rev. Lett.* **2017**, *119*, No. 196001.

(40) Naresh-Kumar, G.; MacIntyre, H.; Subashchandran, S.; Edwards, P. R.; Martin, R. W.; Daivasigamani, K.; Sasaki, K.; Kuramata, A. Origin of Red Emission in B-Ga_2O_3 Analyzed by Cathodoluminescence and Photoluminescence Spectroscopy. *Phys. status solidi* **2021**, *258*, No. 2000465.

(41) Binet, L.; Gourier, D. ORIGIN OF THE BLUE LUMINESCENCE OF β-Ga_2O_3. *J. Phys. Chem. Solids* **1998**, *59*, 1241−1249.

(42) Varley, J. B.; Weber, J. R.; Janotti, A.; Van De Walle, C. G. Oxygen Vacancies and Donor Impurities in β-Ga_2O_3. *Appl. Phys. Lett.* **2010**, *97*, 97−100.

(43) Ryou, H.; Yoo, T. H.; Yoon, Y.; Lee, I. G.; Shin, M.; Cho, J.; Cho, B. J.; Hwang, W. S. Hydrothermal Synthesis and Photocatalytic Property of Sn-Doped β-Ga_2O_3 Nanostructure. *ECS J. Solid State Sci. Technol.* **2020**, *9*, No. 045009.

(44) Choi, B.; Allabergenov, B.; Lyu, H.-K.; Lee, S. E. Twin-Induced Phase Transition from β-Ga_2O_3 to α-Ga_2O_3 in Ga_2O_3 Thin Films. *Appl. Phys. Express* **2018**, *11*, No. 061105.